DINAME 2019 - Proceedings of the XVIII International Symposium on Dynamic Problems of Mechanics,
M.A. Savi, T.G. Ritto and W.M. Bessa (Editors), ABCM, Buzios, RJ, Brazil, March 10th to 15th, 2019

Dynamics of Tethered Multicopters Including an Improved Tether Model

Davi F. de Castro[1], **Igor Afonso A. Prado**[1], **Mauricio Andrés V. Morales**[1] **and Domingos A. Rade**[1]

[1] ITA - Aeronautics Institute of Technology, Division of Mechanical Engineering, São José dos Campos, Brazil

Abstract: This paper addresses the three-dimensional dynamic modeling of tethered multicopters including improvements in the model of the tether, which is assumed to be composed of an arbitrary number of rigid links interconnected through joints rotational joints. These later concentrate the mass, bending stiffness and viscous damping of the tether. After adequate parameterization, the equations of motion are derived for a multicopter using Lagrangian formulation. Simulations are performed on MATLAB/Simulink to evaluate the performance of the tethered multicopter in reaching hover position.

Keywords: Tethered multicopter, dynamic modeling, MAV, UAV

INTRODUCTION

Multicopter Aerial Vehicle (MAVs) have been the subject of many academic studies and have attracted much attention from industry in recent years. MAVs have flight capabilities such as hovering, Vertical Take-Off and Landing (VTOL) and agile maneuvering capabilities, which cannot be achieved by conventional fixed wing aircraft (Bouabdallah *et al.*, 2004). On the other hand, a typical drawback of multicopter vehicles is their reduced endurance, which hardly exceeds some minutes (Bresciani, 2008). Hence, tethered MAVs, featuring a tether connecting them to the ground or to another device, have been introduced as a possible means of circumventing this limitation. Despite limiting the vehicle flight range, the tether can be used for data transmission and power supply during operation, which improves the vehicle endurance. In the scope of modeling and control of tethered multicopters, the work of Castro *et al.* (2015) presented a modeling and hover control strategy for tethered multicopters. In order to reproduce the tether dynamic behavior, a simplified massless viscously damped model was considered for the cable. The hover control strategy was based on a saturated state feedback, and a comparison between free and tethered flight was presented. Using the same approach for the tethered multicopter, Castro *et al.* (2016b) presented a position control for an octocopter. An improved tether model was used in (Castro *et al.*, 2016a) for a hovering analysis of a tethered multicopter under external disturbances. The cable consisted of a series of elastic elements with the mass elements lumped at the nodes. The drag force acting on both vehicle frame and tether was taken into consideration. Regarding the derivation of the mathematical model, most researchers adopt the Newton-Euler continuous-time formulation for the vehicle and tether (Tognon and Franchi, 2015a,b; Nicotra *et al.*, 2014). However, these models are commonly based on two simplifying assumptions, namely, that the multicopter and the tether remain in a fixed plane, and that the tether remains stretched. In addition, energy dissipation (damping) associated to the cable deformation is often neglected. As a result, these models may not be suitable for realistic maneuvering scenarios, such as aggressive translations and rotations, cannot account for three-dimensional deformations of the tether due to dynamic coupling with the multicopter, and cannot represent correctly the motion decay induced by dissipative effects. In contrast to previous works on tethered MAV, this paper focuses on eliminating the aforementioned restrictive assumptions of the dynamic model of the tether. In this way, a three-dimensional dynamic model is derived for the tethered system in which the tether is composed of an arbitrary number of rigid links that are interconnected through joints containing rotational springs and dampers, which are activated by the relative motion between two adjacent links. The mathematical model is obtained through continuous-time Lagrangian formulation. Simulations are run on MATLAB/Simulink environment to evaluate the performance of the tethered MAV in reaching hover position.

DERIVATION OF THE DYNAMIC MODEL OF A TETHERED MULTICOPTER

Consider a multicopter connected to the ground via a tether, as illustrated in Figure 1. The tether is modeled as a serial connection of an arbitrary number of links, n, whose lengths are indicated by l_i, $i = 1,2...,n$. The interconnection between two adjacent links is modeled as a linear spring-viscous damper system (k_j, c_j), $j = 0,1,2,...n-1$, which exert moments proportional to the relative rotation angles and time derivatives of these angles. It should be clarified that, in spite of the simplified representation of the joints in Figure 1, the springs and dampers introduce moments in two mutually orthogonal directions when two successive links rotate with respect to each other.

The inertial frame is defined by the unit vectors $\mathbf{e}_1 = [1\ 0\ 0]^{\mathrm{T}}$, $\mathbf{e}_2 = [0\ 1\ 0]^{\mathrm{T}}$ and $\mathbf{e}_3 = [0\ 0\ 1]^{\mathrm{T}} \in \mathbb{R}^3$. The third axis $\mathbf{e}_3$ is oriented in the local vertical to the direction. In addition, a body-fixed reference frame $\{\mathbf{b}_1, \mathbf{b}_2, \mathbf{b}_3\}$ is defined such that its origin is located at the center of mass of the multicopter, and is oriented as shown in Fig. 1.

The location of the mass center, and the attitude of the multicopter are denoted by $\mathbf{r} \in \mathbb{R}^3$ and $\mathbf{R} \in \mathsf{SO}(3)$, respectively, where the special orthogonal group is $\mathsf{SO}(3) = \{\mathbf{R} \in \mathbb{R}^{3\times 3} \mid \mathbf{R}^{\mathrm{T}}\mathbf{R} = I_{3\times 3}, \det[\mathbf{R}] = 1\}$. A rotation matrix $\mathbf{R}$ represents the linear transformation of a vector from the body-fixed frame to the inertial frame. The Euler angles representation for attitude parameterization is adopted here.

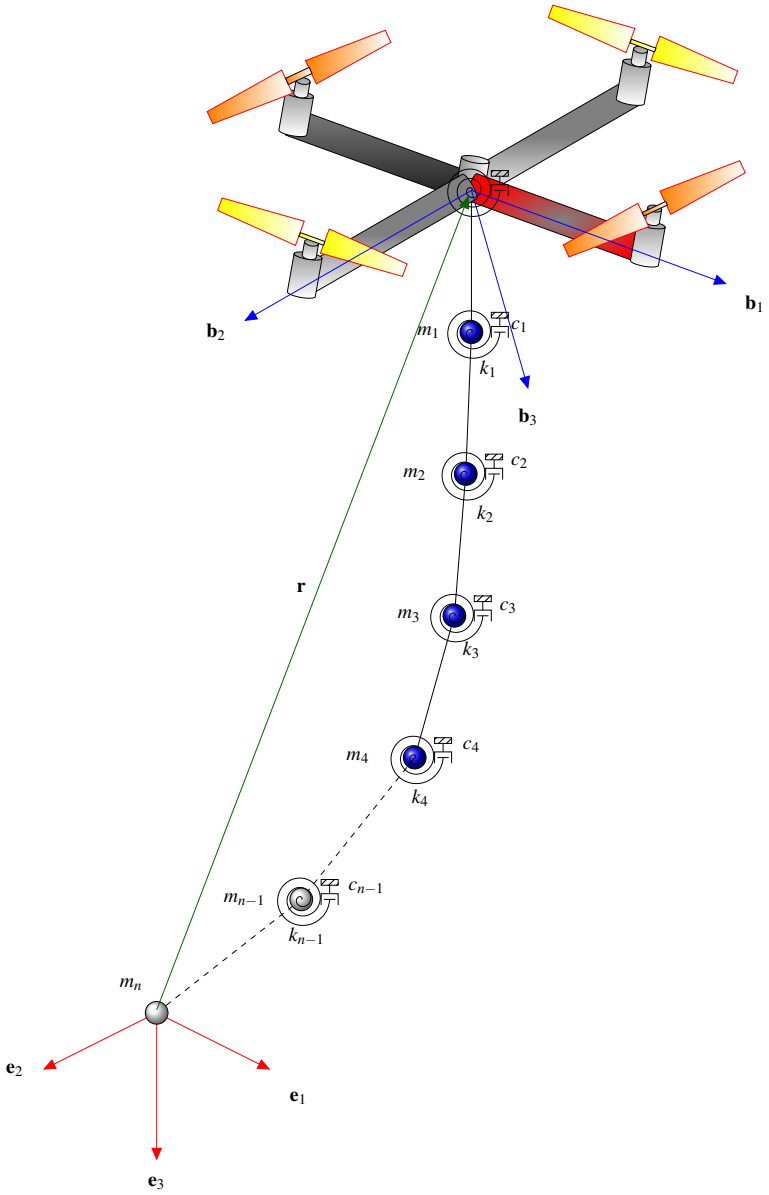

Figure 1: Tethered multicopter.

The mass and the inertia matrix of the multicopter are denoted by $m \in \mathbb{R}$ and $\mathbf{J} \in \mathbb{R}^{3\times 3}$, respectively. The multicopter propulsion system can generate a thrust $-f\mathbf{R}\mathbf{e}_3 \in \mathbb{R}^3$ with respect to the inertial frame, where $f \in \mathbb{R}$ is the total thrust magnitude. It also generates moments $\mathbf{M} \in \mathbb{R}^3$ with respect to the body-fixed frame.

Let $\mathbf{q}_i \in \mathsf{S}^2$ be the unit-vector representing the direction of the i-th link, where the two-sphere is the manifold of unit-vectors in $\mathbb{R}^3$, i.e., $\mathsf{S}^2 = \{\mathbf{q}_i \in \mathbb{R}^3 \mid \|\mathbf{q}_i\| = 1\}$. The mass of each link is assumed to be concentrated at the outboard end of the link, and the first link is attached to the multicopter center of mass. The mass and length of each i-th are denoted by $m_i \in \mathbb{R}$ and $l_i \in \mathbb{R}$, respectively. The corresponding configuration manifold of this system is $\mathsf{SO}(3) \times \mathbb{R}^3 \times (\mathsf{S}^2)^n$.

The hat map $\hat{\cdot} : \mathbb{R}^3 \to \mathfrak{so}(3)$ is defined by the condition that $\hat{\mathbf{x}}\mathbf{y} = \mathbf{x} \times \mathbf{y}$ for any $\mathbf{x}, \mathbf{y} \in \mathbb{R}^3$, and it transforms a vector in $\mathbb{R}^3$ to a 3×3 skew-symmetric matrix. Finally, the dot product is denoted by $\mathbf{x} \cdot \mathbf{y} = \mathbf{x}^{\mathrm{T}}\mathbf{y}$.

Let $\mathbf{\Omega} \in \mathbb{R}^3$ be the angular velocity of the multicopter represented with respect to the body-fixed frame, and let $\mathbf{\Omega}_i \in \mathbb{R}^3$ be the angular velocity of the i-th link represented with respect to the inertial-frame. This angular velocity is normal to the direction of the link, i.e., $\mathbf{q}_i \cdot \mathbf{\Omega}_i = 0$. Then, the kinematic equations are expressed as

$$\dot{\mathbf{R}} = \mathbf{R}\hat{\boldsymbol{\Omega}}, \tag{1}$$

$$\dot{\mathbf{q}}_i = \boldsymbol{\omega}_i \times \mathbf{q}_i. \tag{2}$$

Aiming at using Lagrange's Equations to derived the differential equations of motion, the kinetic and potential energies, as well the virtual work of the external and non-conservative forces and moments must be formulated.

Kinetic energy

The kinetic energy of the multicopter is given by

$$\mathcal{K}_m = \frac{1}{2}m\|\dot{\mathbf{r}}\|^2 + \frac{1}{2}\boldsymbol{\Omega}^{\mathrm{T}}\mathbf{J}\boldsymbol{\Omega}. \tag{3}$$

Let $\mathbf{r}_i \in \mathbb{R}^3$ be the location of m_i in the inertial frame, which can be written as

$$\mathbf{r}_i = \mathbf{r} + \sum_{a=1}^{i} l_a \mathbf{q}_a. \tag{4}$$

The kinetic energy of the links is given by

$$\mathcal{K}_l = \frac{1}{2}\sum_{i=1}^{n} m_i \|\dot{\mathbf{r}} + \sum_{a=1}^{i} l_a \dot{\mathbf{q}}_a\|^2 \tag{5}$$

After algebraic manipulations, the total kinetic energy can be written as

$$\mathcal{K} = \frac{1}{2}M_{00}\|\dot{\mathbf{r}}\|^2 + \dot{\mathbf{r}} \cdot \sum_{i=1}^{n} M_{0i}\dot{\mathbf{q}}_i + \frac{1}{2}\sum_{i,j=1}^{n} M_{ij}\dot{\mathbf{q}}_i \cdot \dot{\mathbf{q}}_j + \frac{1}{2}\boldsymbol{\Omega}^{\mathrm{T}}\mathbf{J}\boldsymbol{\Omega} \tag{6}$$

where the inertia values $M_{00}, M_{0i}, M_{ij} \in \mathbb{R}$ for $1 \leq i, j \leq n$, are given by

$$M_{00} = m + \sum_{i=1}^{n} m_i; \;\; M_{0i} = \sum_{a=1}^{n} m_a l_i, \; M_{0i} = M_{i0}; \;\; M_{ij} = \left\{ \sum_{a=\max\{i,j\}}^{n} m_a \right\} l_i l_j. \tag{7}$$

Potential energy

The potential energy, including gravitational and elastic contributions, is given by

$$\mathcal{V} = -mg\mathbf{r} \cdot \mathbf{e}_3 - \sum_{i=1}^{n} m_i g \mathbf{r}_i \cdot \mathbf{e}_3 + \frac{1}{2}\sum_{i=1}^{n} (\vartheta_i - \vartheta_{i+1})^2 k_i, \tag{8}$$

where k_i are the stiffness coefficients of the springs and g is acceleration of gravity. As a particular case, all joints can be considered to have a same stiffness coefficient, thus the k_i value will be replaced by K. The angles ϑ_i and ϑ_{i+1} are the angles between links i and $i+1$, as can be seen in Figure 2.

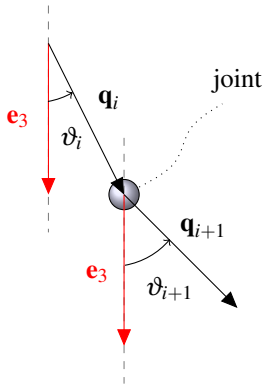

$$\vartheta_i = \cos^{-1}\frac{\mathbf{q}_i.\mathbf{e}_3}{\|\mathbf{q}_i\|\|\mathbf{e}_3\|}$$

$$\vartheta_{i+1} = \cos^{-1}\frac{\mathbf{q}_{i+1}.\mathbf{e}_3}{\|\mathbf{q}_{i+1}\|\|\mathbf{e}_3\|}$$

Figure 2: Angles between two consecutive links.

Given that $\|\mathbf{q}_i\|\|\mathbf{e}_3\| = 1$ and $\|\mathbf{q}_{i+1}\|\|\mathbf{e}_3\| = 1$, after some algebraic manipulation, the potential energy is expressed as

$$\begin{aligned}\mathcal{V} = &-\sum_{i=1}^{n}\sum_{a=i}^{n} m_a g l_i \mathbf{e}_3\cdot\mathbf{q}_i - M_{00} g \mathbf{e}_3\cdot\mathbf{r} + \frac{1}{2}K\sum_{i=1}^{n}\left[\cos^{-1}(\mathbf{q}_i\cdot\mathbf{e}_3)\right]^2 \\ &-K\sum_{i=1}^{n}\left[\cos^{-1}(\mathbf{q}_i\cdot\mathbf{e}_3)\right]\left[\cos^{-1}(\mathbf{q}_{i+1}\cdot\mathbf{e}_3)\right] + \frac{1}{2}K\sum_{i=1}^{n}\left[\cos^{-1}(\mathbf{q}_{i+1}\cdot\mathbf{e}_3)\right]^2\end{aligned} \tag{9}$$

Lagrangian

The Lagrangian of the system is

$$\begin{aligned}\mathcal{L} = \mathcal{K} - \mathcal{V} = &\frac{1}{2}M_{00}\|\dot{\mathbf{r}}\|^2 + \dot{\mathbf{r}}\cdot\sum_{i=1}^{n} M_{0i}\dot{\mathbf{q}}_i + \frac{1}{2}\sum_{i,j=1}^{n} M_{ij}\dot{\mathbf{q}}_i\cdot\dot{\mathbf{q}}_j + \frac{1}{2}\boldsymbol{\Omega}^{\mathrm{T}}\mathbf{J}\boldsymbol{\Omega} \\ &+\sum_{i=1}^{n}\sum_{a=i}^{n} m_a g l_i \mathbf{e}_3\cdot\mathbf{q}_i + M_{00} g \mathbf{e}_3\cdot\mathbf{r} + K\sum_{i=1}^{n}\left[\cos^{-1}(\mathbf{q}_i\cdot\mathbf{e}_3)\right]^2 \\ &-K\sum_{i=1}^{n}\left[\cos^{-1}(\mathbf{q}_i\cdot\mathbf{e}_3)\right]\left[\cos^{-1}(\mathbf{q}_{i+1}\cdot\mathbf{e}_3)\right] + \frac{1}{2}K\sum_{i=1}^{n}\left[\cos^{-1}(\mathbf{q}_{i+1}\cdot\mathbf{e}_3)\right]^2\end{aligned} \tag{10}$$

Equations of motion

The Extended Hamilton's Principle is given by

$$\int_{t_0}^{t_f}\delta\mathcal{L}dt + \int_{t_0}^{t_f}\delta W dt = 0 \tag{11}$$

where

$$\delta\mathcal{L} = \frac{\partial\mathcal{L}}{\partial\mathbf{r}}\cdot\delta\mathbf{r} + \frac{\partial\mathcal{L}}{\partial\mathbf{q}_i}\cdot\delta\mathbf{q}_i + \frac{\partial\mathcal{L}}{\partial\boldsymbol{\Omega}}\cdot\delta\boldsymbol{\Omega} + \frac{\partial\mathcal{L}}{\partial\dot{\mathbf{r}}}\cdot\delta\dot{\mathbf{r}} + \frac{\partial\mathcal{L}}{\partial\dot{\mathbf{q}}_i}\cdot\delta\dot{\mathbf{q}}_i \tag{12}$$

and δW is the virtual work of the non-conservative forces and moments.

The expression for the infinitesimal variation of $\mathbf{q}_i \in \mathsf{S}^2$ should be carefully developed, since the configuration manifold is not a linear vector space. Hence, the infinitesimal variation of $\mathbf{q}_i \in \mathsf{S}^2$ is given by

$$\delta\mathbf{q}_i = \boldsymbol{\xi}_i \times \mathbf{q}_i \tag{13}$$

where $\boldsymbol{\xi}_i \in \mathbb{R}^3$ is constrained to be orthogonal to $\mathbf{q}_i$, i.e., $\boldsymbol{\xi}_i\cdot\mathbf{q}_i = 0$. Similarly, the variation of the angular velocity is given by

$$\delta\Omega = \dot{\boldsymbol{\eta}} + \boldsymbol{\Omega}\times\boldsymbol{\eta} \tag{14}$$

where $\boldsymbol{\eta} \in \mathbb{R}^3$. These expressions are the key element to obtaining global equations of motion on $(\mathsf{S}^2)^n$.

The virtual work of the propulsion force and moment and of the dissipative moments exerted by the cable dampers is given by

$$\begin{aligned}\delta W &= -f\mathbf{R}\mathbf{e}_3\cdot\delta\mathbf{r} - M\cdot\boldsymbol{\eta}dt + c_i(\dot{\vartheta}_i - \dot{\vartheta}_{i+1})(\delta\vartheta_i - \delta\vartheta_{i+1}) \\ &= -f\mathbf{R}\mathbf{e}_3\cdot\delta\mathbf{r} - M\cdot\boldsymbol{\eta} - c_i\left[\frac{-\mathbf{e}_3\dot{\mathbf{q}}_i}{\sqrt{1-(\mathbf{e}_3\cdot\mathbf{q}_i)^2}} + \frac{-\mathbf{e}_3\dot{\mathbf{q}}_{i+1}}{\sqrt{1-(\mathbf{e}_3\cdot\mathbf{q}_{i+1})^2}}\right]\left[\frac{-\mathbf{e}_3\dot{\mathbf{q}}_i}{\sqrt{1-(\mathbf{e}_3\cdot\mathbf{q}_i)^2}}\right]\hat{\mathbf{q}}_i\cdot\boldsymbol{\xi}_i\end{aligned} \tag{15}$$

where c_i are the coefficients of viscous damping. All the connections between links are considered to have a same value of the coefficient of viscous damping, which will be denoted by C.

After substitution of the expressions of kinetic energy, potential energy and virtual work of the external and non-conservative forces and moments into Eq.11, and developments according to the rules of Variational Calculus, the equations of motion for the tethered multicopter are obtained as follows:

$$M_{00}\ddot{\mathbf{r}} + \sum_{i=1}^{n} M_{0i}\ddot{\mathbf{q}}_i = -f\mathbf{R}\mathbf{e}_3 + M_{00}g\mathbf{e}_3 \tag{16}$$

$$\mathbf{J}\dot{\boldsymbol{\Omega}} + \boldsymbol{\Omega}\times\mathbf{J}\boldsymbol{\Omega} = \mathbf{M} \tag{17}$$

$$
\begin{aligned}
&-\hat{\mathbf{q}}_i^2(M_{i0}\ddot{\mathbf{r}}+\sum_{j=1}^{n}M_{ij}\ddot{\mathbf{q}}_j)+\sum_{a=i}^{n}m_a g l_i\hat{\mathbf{q}}_i^2\mathbf{e}_3\\
&+2K\beta_i\hat{\mathbf{q}}_i^2\mathbf{e}_3-K\beta_{i+1}\hat{\mathbf{q}}_i^2\mathbf{e}_3+C\gamma_1\hat{\mathbf{q}}_i^2\mathbf{e}_3+C\gamma_{i+1}\hat{\mathbf{q}}_i^2\mathbf{e}_3=0
\end{aligned}
\tag{18}
$$

where $\beta_i=\dfrac{\cos^{-1}(\mathbf{q}_i\cdot\mathbf{e}_3)}{\sqrt{1-(\mathbf{q}_i\cdot\mathbf{e}_3)^2}}$, $\beta_{i+1}=\dfrac{\cos^{-1}(\mathbf{q}_{i+1}\cdot\mathbf{e}_3)}{\sqrt{1-(\mathbf{q}_{i+1}\cdot\mathbf{e}_3)^2}}$, $\gamma_i=\dfrac{-\mathbf{e}_3\dot{\mathbf{q}}_i}{\sqrt{1-(\mathbf{e}_3\cdot\mathbf{q}_i)^2}}$ and $\gamma_{i+1}=\dfrac{-\mathbf{e}_3\dot{\mathbf{q}}_{i+1}}{\sqrt{1-(\mathbf{e}_3\cdot\mathbf{q}_{i+1})^2}}$. Equation 18 is rewritten to obtain an explicit expression for $\ddot{\mathbf{q}}_i$. As $\mathbf{q}_i\cdot\dot{\mathbf{q}}_i=0$, one obtains $\dot{\mathbf{q}}_i\cdot\dot{\mathbf{q}}_i+\mathbf{q}_i\cdot\ddot{\mathbf{q}}_i=0$. Hence, one obtains

$$
-\hat{\mathbf{q}}_i^2\ddot{\mathbf{q}}_i=-(\mathbf{q}_i\cdot\ddot{\mathbf{q}}_i)\mathbf{q}_i+(\mathbf{q}_i\cdot\mathbf{q}_i)\ddot{\mathbf{q}}_i=(\dot{\mathbf{q}}_i\cdot\dot{\mathbf{q}}_i)\mathbf{q}_i+\ddot{\mathbf{q}}_i,
\tag{19}
$$

substituting Eq. 19 into Eq. 18, one obtains

$$
\begin{aligned}
M_{ii}\ddot{\mathbf{q}}_i-\hat{\mathbf{q}}_i^2(M_{i0}\ddot{\mathbf{r}}+\sum_{j=1,j\neq i}^{n}M_{ij}\ddot{\mathbf{q}}_j)=&-M_{ii}\|\dot{\mathbf{q}}_i\|^2q_i-\sum_{a=i}^{n}m_a g l_i\hat{\mathbf{q}}_i^2\mathbf{e}_3\\
&-2K\beta_i\hat{\mathbf{q}}_i^2\mathbf{e}_3+K\beta_{i+1}\hat{\mathbf{q}}_i^2\mathbf{e}_3-C\gamma_i\hat{\mathbf{q}}_i^2\mathbf{e}_3-C\gamma_{i+1}\hat{\mathbf{q}}_i^2\mathbf{e}_3
\end{aligned}
\tag{20}
$$

Finally, Eqs. 16 and 20 can be cast in a matrix form as follows:

$$
\begin{aligned}
&\begin{bmatrix}
M_{00} & -M_{01} & -M_{02} & \cdots & -M_{0n}\\
-\hat{\mathbf{q}}_1^2M_{10} & M_{11}I_3 & -M_{12}\hat{\mathbf{q}}_1 & \cdots & -M_{1n}\hat{\mathbf{q}}_1^2\\
\hat{\mathbf{q}}_2^2M_{20} & -M_{21}\hat{\mathbf{q}}_2^2 & M_{22}I_3 & \cdots & -M_{2n}\hat{\mathbf{q}}_2^2\\
\vdots & \vdots & \vdots & \ddots & \vdots\\
\hat{\mathbf{q}}_n^2M_{n0} & -M_{n1}\hat{\mathbf{q}}_n^2 & -M_{n2}\hat{\mathbf{q}}_n^2 & \cdots & M_{nn}I_3
\end{bmatrix}
\begin{bmatrix}
\ddot{\mathbf{r}}\\ \ddot{\mathbf{q}}_1\\ \ddot{\mathbf{q}}_2\\ \vdots\\ \ddot{\mathbf{q}}_n
\end{bmatrix}\\
&=\begin{bmatrix}
-f\mathbf{R}\mathbf{e}_3+M_{00}g\mathbf{e}_3\\
-||\dot{\mathbf{q}}_1||^2M_{11}\mathbf{q}_1-\sum_{a=1}^{n}m_a g l_1\hat{\mathbf{q}}_1^2\mathbf{e}_3-2K\beta_1\hat{\mathbf{q}}_1^2e_3+K\beta_2\hat{\mathbf{q}}_1^2\mathbf{e}_3-C\gamma_1\hat{\mathbf{q}}_1^2\mathbf{e}_3-C\gamma_2\hat{\mathbf{q}}_1^2\mathbf{e}_3\\
-||\dot{\mathbf{q}}_2||^2M_{22}\mathbf{q}_2-\sum_{a=2}^{n}m_a g l_2\hat{\mathbf{q}}_2^2\mathbf{e}_3-2K\beta_2\hat{\mathbf{q}}_2^2\mathbf{e}_3+K\beta_3\hat{\mathbf{q}}_2^2\mathbf{e}_3-C\gamma_2\hat{\mathbf{q}}_2^2\mathbf{e}_3-C\gamma_3\hat{\mathbf{q}}_2^2\mathbf{e}_3\\
\vdots\\
-||\dot{\mathbf{q}}_n||^2M_{nn}\mathbf{q}_n-m_n g l_n\hat{\mathbf{q}}_n^2\mathbf{e}_3-2K\beta_n\hat{\mathbf{q}}_n^2\mathbf{e}_3-C\gamma_n\hat{\mathbf{q}}_i^2\mathbf{e}_3
\end{bmatrix}
\end{aligned}
\tag{21}
$$

NUMERICAL SIMULATIONS

Here are presented numerical simulations of the tethered multicopter in hovering flight. The equations of motion were integrated with a fourth-order Runge-Kutta algorithm with time step of T = 0.002 s. The simulation was run for 10 seconds. The initial direction of the links was chosen so that the cable is oriented along the horizontal direction, which means that the angles ϑ_i are 90° for all the links. In addition, the initial angular velocity of each link was chosen to be zero. The vehicle was commanded to maintain the initial hover position at $\mathbf{r}=[0\ 0\ 1]^{\mathrm{T}}$m. The parameters adopted in the simulation are presented in Table 1. The control system adopted for the hovering flight is presented in Santos *et al.* (2013) and consists of a Proportional Derivative (PD) controller.

Figure 3 shows the simulation of the angles ϑ_i for each link of the tether, first by assuming the connections between the links without springs nor viscous dampers. Note that, despite the control action, the ϑ_i angles exhibit strong variations and do not achieve steady-state regime.

Figure 4 shows the variations of angles ϑ_i, this time considering the presence of angular springs and dampers at connections between the links. It can be seen that, in spite of strong transient responses in the first 2 seconds of the simulation, cable oscillations are strongly attenuated and steady-state regime is achieve after 4 seconds.

Table 1: Parameters of the tethered MAV.

Items	Parameter	Value	Units
Mass	m	2.132	kg
Acceleration of gravity	g	9.796	m/s^2
Length of arm	l	0.36	m
Moment of inertia on x-axis	J_x	0.043	kg.m^2
Moment of inertia on y-axis	J_y	0.055	kg.m^2
Moment of inertia on z-axis	J_z	0.092	kg.m^2
Mass of the node	m_i	0.1	kg
Number of links	n	2	
Length of link	l_i	0.4	m
Stiffness coefficients	K	0.2	Nm
Damping coefficients	C	0.1	Ns/m

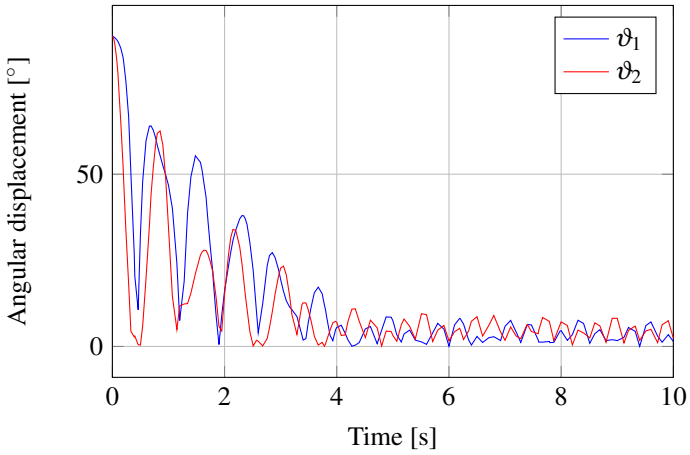

Figure 3: Angular displacement of the tether links without springs nor dampers included in the nodes.

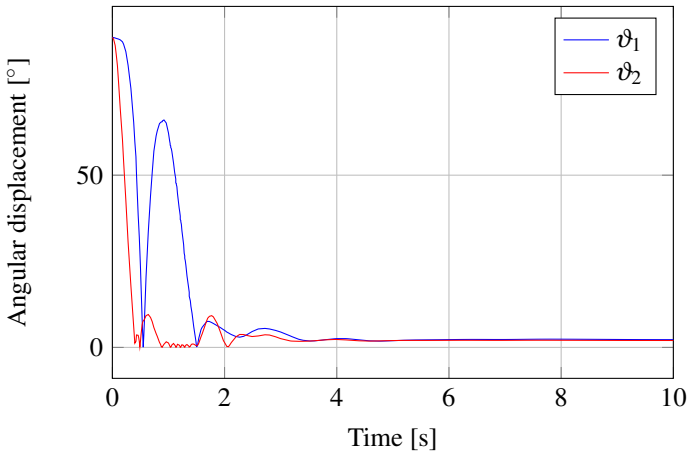

Figure 4: Angular displacement of the tether links with springs and dampers included in the nodes.

CONCLUSIONS

This work has presented the modeling of a tethered multicopter configuration based on the Extended Hamilton Principle. Aiming at improving the capability of mathematical model to reproduce actual conditions, stiffness-damping effects localized at the nodes of the tether were include. Numerical simulations showed that these effects do exert significant influence on the dynamic behavior of the system, especially in terms of the time necessary for achieving steady-state

conditions without any appreciable residual oscillation. Future developments will consider space-continuous models with distributed inertia, stiffness and damping, for representing the tether dynamics.

ACKNOWLEDGMENTS

D.F. de Castro and I.A.A. Prado thank the Brazilian Foundation CAPES the doctorate scholarships granted to them. D.A. Rade gratefully acknowledge the Brazilian Research Council CNPq (Grant number 310633/2013-3 and São Paulo State Research Agency (Grant number 2015/20363-6) for the financial support to his research work. The authors also thank ALTAVE for the partnership in conducting this research.

REFERENCES

Bouabdallah, S., Murrieri, P. and Siegwart, R., 2004. "Design and control of an indoor micro quadrotor". In *IEEE International Conference on Robotics and Automation ICRA*. IEEE. doi:10.1109/robot.2004.1302409.

Bresciani, T., 2008. *Modelling, Identification and Control of a Quadrotor Helicopter*. Master's thesis, Lund University.

Castro, D.F., Prado, I.A.A., de Freitas Virgilio Pereira, M., dos Santos, D.A., Balthazar, J.M. and Morales, M.A.V., 2016a. "Hovering analysis of a tethered multirotor under external disturbances". In *IX Congresso Nacional de Engenharia Mecanica (CONEM)*. Fortaleza, CE, Brazil, pp. 1–9.

Castro, D.F., Prado, I.A.A., de Freitas Virglio Pereira, M., dos Santos, D.A. and Balthazar, J.M., 2016b. "Modeling and position control of tethered octocopters". In *International Conference on Structural Nonlinear Dynamics and Diagnosis (CSNDD)*. MATEC Web of Conferences, Marrakech, Morocco, Vol. 83, pp. 1–4. doi:10.1051/matecconf/20168303001.

Castro, D.F., Santos, J.S., de Oliveira, M.B.X., dos Santos, D.A. and Goes, L.C.S., 2015. "Modeling and control of tethered unmanned multicopters in hovering flight". In *AIAA Aviation*. Aerospace Research Central, Dallas, TX, pp. 1–9. doi:10.2514/6.2015-2333.

Nicotra, M.M., Naldi, R. and Garone, E., 2014. "Taut cable control of a tethered uav". In *World Congress The International Federation of Automatic Control (IFAC)*. Elsevier, Cape Town, South Africa, Vol. 47, pp. 3190–3195. doi:10.3182/20140824-6-ZA-1003.02581.

Santos, D.A., Saotome, O. and Cela, A., 2013. "Trajectory control of multirotor helicopters with thrust vector constraints". In *Mediterranean Conference on Control & Automation (MED)*. IEEE, Platanias-Chania, Crete, Greece, pp. 1–5.

Tognon, M. and Franchi, A., 2015a. "Nonlinear observer-based tracking control of link stress and elevation for a tethered aerial robot using inertial-only measurements". In *IEEE International Conference on Robotics and Automation (ICRA)*. IEEE, Seattle, Washington, pp. 3994–3999. doi:10.1109/ICRA.2015.7139757.

Tognon, M. and Franchi, A., 2015b. "Nonlinear observer for the control of bi-tethered multi aerial robots". In *IEEE/RSJ International Conference on Intelligent Robots and Systems (IROS)*. Hamburg, Germany, pp. 1852–1857. doi:10.1109/IROS.2015.7353619.

RESPONSIBILITY NOTICE

The author(s) is (are) the only responsible for the printed material included in this paper.